Heliyon 10 (2024) e37539

Contents lists available at ScienceDirect

Heliyon

journal homepage: www.cell.com/heliyon

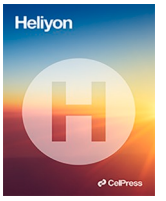

Research article

Use of microalgal-fungal pellets for hydroponics effluent recycling and high-value biomass production

Harshit Tiwari, Sanjeev Kumar Prajapati *

Environment and Biofuel Research Lab (EBRL), Department of Hydro and Renewable Energy, Indian Institute of Technology (IIT) Roorkee, Uttarakhand, 247667, India

ARTICLE INFO

Keywords:
Algal-fungal pellets
Hydroponic effluent
Treatment
Recycling
Biomass
Bioenergy

ABSTRACT

Hydroponic effluent (HE), enriched with inorganic nutrients, presents a viable, low-cost cultivation medium for microalgal biomass production and subsequent resource recovery. However, downstream processing, particularly biomass harvesting, remains a critical challenge for microalgal biorefineries. Therefore, the present study explored the potential of microalgal-fungal pellets (MAFP) in HE recycling for the production of biochemical-rich biomass. The optimized fungi-to-microalgae ratio (F:A) of 1:3 resulted in 100 % microalgal pelletization within 6 h. Surface characteristics suggested that metabolically active fungi with opposite charges facilitate microalgal pelletization. Further, MAFP exhibited a packed porous structure that was resilient to shear forces and had a high capacity for nutrient uptake. MAFP cultivation in HE demonstrated complete removal of ammonia-nitrogen (NH_3-N), phosphate (PO_4^{3-}), and nitrate-nitrogen (NO_3^--N) within 7–9 days. The produced biomass was rich in biomolecules, including lipids (18.36 ± 0.12 % TS), protein (52.06 ± 2.1 % TS), and carbohydrates (28.95 ± 0.05 % TS). Besides, the high methane potential of MAFP (SMP ≈ 502.74 ± 19.1 mL CH_4 g^{-1} VS, and TMP ≈ 817.68 ± 12.5 mL CH_4 g^{-1} VS) indicated its suitability for biogas production. In essence, MAFP offers efficient HE recycling and biochemically rich biomass production, advancing towards a green and circular bioeconomy.

1. Introduction

Water is integral to the sustainable development of any nation, contributing significantly to human and socio-economic progress, energy and food production, ecosystem stability, and human survival. It serves as a fundamental element in climate change adaptation, forming a crucial nexus between society and the environment. As global population and economic expansion continue, water, land, and food resources strain intensifies. The world population is projected to reach 9.7 billion by 2050, necessitating a 70 % increase in food production to meet anticipated demand [1]. In this context, hydroponics technologies emerge as a scientifically advanced solution for the production of high-yield crops with a shorter cultivation time [2,3]. For instance, hydroponics systems increase lettuce yields per acre by up to 20 times [4]. Crop cultivation through hydroponics requires substantial quantities of water and inorganic nutrients (nitrogen and phosphorus). However, only a fraction of the supplied nutrients (20 %–30 %) are utilized by the plants, and residual nutrients end up as HE [5,6]. As the hydroponics market grows rapidly, there are high possibilities of continuous discharge of hydroponic wastes into water bodies, leading to severe water pollution, including eutrophication in surface water bodies and

* Corresponding author. IIT Roorkee, Uttarakhand, 247667, India.
E-mail addresses: sanjukec@hre.iitr.ac.in, sanjukec@gmail.com (S.K. Prajapati).

https://doi.org/10.1016/j.heliyon.2024.e37539
Received 19 June 2024; Received in revised form 7 August 2024; Accepted 4 September 2024
Available online 10 September 2024

groundwater contamination due to direct leaching [7,8]. Considering the potential negative environmental consequences associated with the discharge of untreated HE, significant research endeavors are being made to treat and recycle HE. For example, ultraviolet treatment [9], ultrafiltration coupled reverse osmosis [10], chemical precipitation [7], sand, and microfiltration [7,10]. Nature-based treatments, including constructed wetlands [11] and nitrification-denitrification methods [12], were also explored. However, constructed wetlands demand significant land area and prolonged retention times, while nitrification-denitrification processes can contribute to greenhouse gas emissions through nitrogen gas production [7].

Microalgae cultivation has emerged as a promising avenue for effluent treatment, capitalizing on the ability of microalgae to assimilate and mitigate nutrient-rich wastewater, contributing to a more sustainable and ecologically friendly approach to HE management. Microalgae also provide an opportunity for resource recovery, such as biofuel and other value-added compounds (pigments, microelements, omega fatty acids, antioxidants, and animal feed) from a range of wastewater, including HE [13–15]. Nevertheless, the economic feasibility of harvesting microalgal biomass remains a significant challenge due to the diluted nature (<1 g/L) and small size (<30 μm) of microalgal cells [16]. Harvesting and dewatering of microalgal biomass are particularly expensive, accounting for 20–30 % of total production costs due to high operational costs (0.5–2 € kg^{-1}) and high energy demands (0.2–5 kWh kg^{-1}) [17]. Several mechanical and chemical methods for microalgal biomass harvesting exist, encompassing techniques such as centrifugation, flotation, flocculation, filtration, gravity sedimentation, and electrophoresis [16]. Despite recent advancements, microalgal harvesting remains challenging due to techno-economic constraints. Moreover, microalgal biomass harvesting based on bioagents such as bacteria, fungi, protozoa, and microbial metabolites holds promise in overcoming some of these challenges [18,19]. Filamentous fungi such as *Aspergillus* are efficient in pelletizing various microalgae from the nutrient medium [19]. For example, Prajapati et al. [20] observed that *Aspergillus lentulus* FJ172995 effectively pelletizes *Chroococcus* sp., within 6 h. Likewise, *Aspergillus fumigatus* completely pelletizes *C. pyrenoidosa* within 3 h [21]. Further, utilizing microalgal-fungal pellets (MAFP) in wastewater treatment could also hold promise for enhancing treatment efficacy and facilitating improved resource recovery. Successful implementation of MAFP technology could potentially circumvent the bottleneck associated with microalgal biomass harvesting, thereby enhancing the overall economic viability of microalgal-based biorefineries.

To the best of the author's knowledge, the utilization of microalgal-fungal pellets (MAFP) for HE treatment has not been disclosed so far. Considering the aforementioned research gaps, this study aims to explore *Aspergillus fumigatus*-mediated *Scenedesmus obliquus* pelletization for possible recycling of HE and co-production of biochemical-rich biomass. Initially, F:A was optimized for complete pelletization of microalgal biomass. Besides, underlying possible interactions between microalgae and fungal hyphae were investigated. The optimized MAFP (F:A ≈ 1:3) was subsequently tested for its efficacy in pollutant removal. Following effluent treatment, biochemical and elemental characterization of MAFP was conducted to assess its potential for value-added products and bioenergy generation.

2. Materials and methods

2.1. Microorganisms and growth conditions

Pure culture of *Scenedesmus obliquus* (NCIM 5586) was procured from the National Collection of Industrial Microorganism (NCIM), CSIR-National Chemical Laboratory Pune (NCL-Pune). The microalgal culture was maintained in 1.5 % agar slants supplemented with BG11 media in a fabricated microalgal growth chamber (illuminance 81 μmol m^{-2} s^{-1}, 16/8 h-light/dark, and 25 ± 0.5 °C) [2]. Moreover, liquid culture was maintained in BG11 broth.

Previously isolated *Aspergillus fumigatus* was used for the pelletization of microalgal biomass. The fungal culture was maintained on sterile 1.5 % (w/v) potato dextrose agar slants at 4 ± 0.5 °C in the laboratory refrigerator. The spore suspension was prepared by inoculating a loopfull fungus culture in a sterile broth medium for 3 days under dark conditions. The spore suspension (0.2 mL) was then inoculated in 50 mL medium and incubated at 25 ± 0.5 °C on a rotary incubator at 160 rpm for 24 h to achieve fungal pellets.

2.2. Pelletization experiment

Pelletization of microalgal biomass using fungal pellets was carried out in a 250 mL Erlenmeyer flask with a working volume of 100 mL. The precultured microalgal cells were mixed with overnight grown fungal cells at varying fungal-microalgal ratios (F:A) viz. 1 : 1, 1 : 3, 1 : 6, and 1 : 9 (% dry cell weight) [20,21]. Each flask was then incubated at room temperature (25 ± 0.5 °C) with continuous shaking (120 rpm) in a benchtop orbital shaker until the complete microalgal pellets were formed. Samples were withdrawn periodically, and the absorbance of the liquid broth was measured at 680 nm to quantify microalgal biomass harvesting. Further, the microalgal biomass harvesting, estimated in terms of pelletization efficiency, was expressed as:

$$B_{PE}\ (\%) = \left[1-\frac{OD_{680\ f}}{OD_{680i}}\right] \times 100 \quad (1)$$

where, B_{PE} = Pelletization efficiency at time, OD_{680i} OD_{680f} are the optical density at initial and final time, respectively.

2.3. Microalgal and fungal surface characterization

In order to investigate the interaction between microalgae and fungus during pelletization, the surface properties of both were

examined using a particle size analyzer (HORIBA Scientific nano particle analyzer SZ-100), and Fourier transform infrared spectroscopy measurements (TENSOR II FTIR Routine Spectrometer). The electrostatic charge at the surface of microalgal cells were analyzed using Zeta potential. To perform FTIR measurements, the samples were first rinsed with phosphate-buffered saline (PBS) and then lyophilized using a Labogene CoolSafe tabletop freeze dryer. The resulting lyophilized samples were then subjected to Fourier transform infrared (FTIR) spectroscopy analysis using a TENSOR II FTIR Routine Spectrometer (Cat. No. BOPT TENSOR)

2.4. Physical and mechanical properties of microalgal-fungal pellets

Once the MAFP was formed, its physical properties, such as diameter and sphericity, were examined. The diameter of the MAFP was calculated by averaging the shortest and longest diameters, while the sphericity was calculated as the percentage ratios of the shortest and longest diameters [22]. Besides, morphological analysis of MAFP was performed using Field Emission Scanning Electron Microscopy (FE-SEM; Zeiss Gemini 300).

The mechanical properties, such as density and detachment rate of MAFP, were determined following the procedure reported elsewhere [23]. For the determination of density, the excess moisture of the MAFP was initially absorbed using filter paper, and the weight was recorded. Subsequently, MAFP and distilled water were placed in a 10 mL measuring graduated cylinder, and the total volume of pellets and the distilled water was recorded. The density of the MAFP was then calculated following equation (2).

$$\rho = \frac{w_p}{(v_2\text{-}v_1)} \tag{2}$$

where, w_p is the weight of fungal microalgal pellets (g), V_1, and V_2 are the volume of distilled water (mL), and the total volume of fungal microalgal pellets plus distilled water (mL), respectively.

The detachment rate of microalgae from MAFPs were evaluated following the procedure described elsewhere [23]. Ten pellets of MAFP were added in a 100 mL Erlenmeyer flask containing 10 mL of distilled water and incubated for 9 days at 25 ± 0.5 °C under continuous shaking at 120 rpm. The number of detached pellets was then recorded and calculated according to equation (3).

$$\textit{Detachment rate}\ \% = \frac{N_f}{10} \times 100 \tag{3}$$

where, N_f, is the number of microalgae detached pellets after 9 d incubation.

2.5. Pollutant uptake assessment from hydroponics effluent using microalgal-fungal pellets

The HE was collected from a hydroponics farm located in Uttarakhand, India. The collected effluent was analyzed for its physicochemical parameters following the standard protocols as mentioned elsewhere [2]. The phycoremediation potential of tested MAFP was carried out in 250 mL Erlenmeyer flask using an inoculum of 50 pellets per 50 mL [24]. All the experimental flasks were incubated under laboratory-controlled conditions in a fabricated microalgal growth chamber with an illumination of 81 μmol m^{-2} s^{-1}, a light/dark cycle of 16/8 h, a shaking speed of 120 rpm, and a temperature of 25 °C. Besides, the flasks with only fungal pellets as well as flasks with only microalgae, were used as controls. Samples were collected periodically to assess the residual concentrations of pollutants (NH_3-N, NO_3^--N, and PO_4^{3-}). Subsequently, the pollutant uptake rates (mg L^{-1} d^{-1}), and pollutant uptake efficiency (PE) were calculated following equation (4), and (5).

$$P_r = \frac{p_0\text{-}p_t}{t_0\text{-}t_t} \tag{4}$$

$$PE\ \% = \left(1\text{-}\frac{p_t}{p_0}\right) \times 100 \tag{5}$$

where, P_r represents the pollutant uptake rate; p_0 is the initial pollutant concentration (NO_3^-, PO_4^-), and p_t is the pollutant concentration after treatment at time t.

2.6. Downstream processing of microalgal-fungal pellets

2.6.1. Ultimate analysis of microalgal-fungal pellets

The elemental composition of MAFP and microalgae was determined using a CHNS/O analyzer. Briefly, 2 mg of dried biomass was combusted at 1000 °C to produce mixtures of gases. The gases were then passed through the absorbent traps to remove additional gases and leave only CO_2, SO_2, H_2O, and N_2 gases. Subsequently, the collected gases were allowed to be separated and measured using GC column chromatography equipped with a thermal conductivity detector (TCD). Further, the elements were quantified by calibrating each component using high-purity micro-analytical standards [2].

2.6.2. Stoichiometric calorific energy value and maximum biomethane production potential of microalgal-fungal pellets

The maximum theoretical energy potential of microalgal-fungal pellets biomass was estimated by calculating the stoichiometric calorific energy value (CEV) following equation (6) adopted from Channiwala and Parikh [25].

$$\text{CEV MJ Kg}^{-1} = 0.349\ \text{C} + 1.1783\ \text{H} - 0.1034\ \text{O} - 0.015\ \text{N} - 0.0211\ \text{A} \quad (6)$$

where C, H, N, O, and A represent the mass (% TS)of carbon, hydrogen, nitrogen, oxygen and ash content, respectively.

The maximum possible biomethane potential of tested microalgal-fungal pellets biomass was estimated in terms of Stochiometric methane potential (SMP) and Theoretical methane potential. (TMP), following Symons and Buswell [26] equations derived from Prajapati et al. [27].

$$H_yO_zN_\alpha + \left[\frac{4x-y-2z+3\alpha}{4}\right]H_2O \rightarrow \left[\frac{4x+y-2z-3\alpha}{8}\right]CH_4 + \left[\frac{4x-y+2z+3\alpha}{8}\right]CO_2 + \alpha NH_3 \quad (7)$$

$$SMP = \left[\frac{4x+y-2z-3\alpha}{96x+8y+128z+112\alpha}\right]V_{CH_4} \quad (8)$$

where, x, y, z, and α are the stoichiometric coefficients of Carbon (%), Hydrogen (%), Oxygen (%), and Nitrogen (%), respectively, and V_{CH4} is the molar volume of biomethane in STP.

$$TMP = \frac{1}{100}[\alpha \times L + \beta \times P + \gamma \times C] \quad (9)$$

where, α, β, and γ are the specific biomethane yields of lipids (1.014 L CH_4 g^{-1} VS), protein (0.851 L CH_4 g^{-1} VS), and carbohydrates (0.415 L CH_4 g^{-1} VS), respectively; Moreover, L, P, and C are the mass (% TS) of lipids, protein, and carbohydrates, respectively.

2.6.3. Cell disruption

To extract biomolecules such as carbohydrates, lipids, and proteins from the MAFP biomass, we have adopted two cell disruption methods such as acid pretreatment (2.5 N HCl) and microwave-assisted pretreatment (700 W for 5 min), for the estimation of carbohydrates and lipids, respectively [28,29]. Besides, protein content was estimated by multiplying the elemental nitrogen content (N %) of the dried biomass with nitrogen to protein conversion factor (N/P ≈ 6.25) [30].

2.6.4. Carbohydrates and lipid estimation

For carbohydrate estimation, a modified phenol sulfuric acid method was adopted. Briefly, 0.1 mL of supernatant from acid-pretreated microalgal biomass was taken into a clean test tube and diluted to 1 mL using HQ-pure water. After that, 1 mL of phenol solution (5 % w/v), followed by 5 mL of concentrated sulfuric acid, was added to the diluted sample and incubated for 10–20 min at room temperature. A reddish-brown color was developed, indicating carbohydrate presence in the test sample. For the estimation of absolute carbohydrate concentration, the absorbance of each test sample was recorded at 490 nm using a spectrophotometer (PerkinElmer, UV/VIS Lamda 365). The concentration of carbohydrates (mg L^{-1}) was determined by using a pre-developed calibration equation (10), as mentioned elsewhere [30].

$$\text{Glucose concentration } (mg.L^{-1}) = \frac{Ab_{490} - 0.0167}{0.0107} \quad (R^2 = 0.99) \quad (10)$$

where, Ab $_{490}$ is the absorbance at 490 nm.

For lipid estimation, Bligh and Dyer's method was used [31]. After microwave treatment of biomass, add chloroform and methanol (1:2) to them and mix continuously for 1 h using an orbital shaker (Scigenics Biotech Le 4676-ah) at 200 rpm. Subsequently, 5 mL of HQ-pure water was added to the mixed solution, and the suspension was kept static until the organic phase was separated. The organic phase (lipids) from the mixture was then carefully withdrawn into a clean test tube, and the amount of extracted lipid was recorded (V). Besides, the known volume (v) of the organic phase was placed in pre-weighted aluminum foil cups and then oven-dried at 105 °C until chloroform completely evaporated. Lastly, the weight of dried aluminum foil cups was noted, and the absolute amount of lipid was quantified using equation (11).

$$\text{Lipid } (mg) = \frac{(w_f - w_i)}{v} \times V \quad (11)$$

where, w_i and w_f are the initial, and final weight of the aluminum foil cups in mg, respectively; V and v are the total volume of organic phase containing lipid, and the aliquot volume, respectively.

2.7. Statistical analysis

All experiments were carried out in triplicates. The results are represented as Mean ± Standard deviation and error bars in the graphs.

3. Result and discussion

3.1. F:A ratios impact the microalgal biomass pelletization

The variation in pelletization efficiency (B_{PE}) at tested F:A ratios are shown in Fig. 1. It was well observed that the graph of B_{PE} exhibited a sigmoidal curve with no lag phase. During the first 0.5 h of the experiment, no significant changes were observed in all the experimental sets ($B_{PE} \leq 20$ %). However, from 0.5 h onwards, the difference in B_{PE} at various F:A ratios was observed. For instance, among all the experimental sets, F:A ratio 1 : 1 showed complete microalgal pelletization ($B_{PE} \approx 100$ %) within 3 h. Besides, 1 : 3 F:A ratio, showed 82.01 % B_{PE} within 3 h, and complete pelletization was observed at 6 h. Hence, it can be said that rapid microalgal pelletization was observed in both F:A ratios (1 : 1, and 1 : 3). Further, no pelletization was observed in the control sets (only microalgae). The variation might be predominantly attributed to the duration of adaptation and synthesis of extracellular polymeric substances (EPS) by microalgae or fungi [32]. As time progresses, microbial growth and EPS production increase, facilitating particle aggregation and the formation of larger, and more efficient pellets [33,34]. This leads to improved B_{PE} over time as the system stabilizes. The B_{PE} was saturated after some time, and the curve levels off in a plateau phase, which indicates that the maximum B_{PE} has been achieved.

On the other hand, totally different microalgal pelletization profiles were observed with F:A ratios below 1 : 3. For example, both 1 : 6, and 1 : 9 F:A showed rapid attachment of microalgal biomass till 6 h of incubation with B_{PE} of 71.15 %, and 58.10 %, respectively. However, 6 h onwards, the pelletization rate for both ratios slowed down. Interestingly, ≈90 % B_{PE} was also achieved at an F:A 1 : 6, but it required a significantly longer incubation time (24 h) compared to F:A ratios <1 : 3. In addition, at an F:A 1 : 9 did not achieve complete pelletization till 24 h ($B_{PE} \approx 70.65$ %). The poor B_{PE} for F:A ratio 1 : 6, and 1 : 9 indicates that the fungi used in these cases were insufficient to achieve complete microalgal pelletization. Overall, from the above results, it can be seen that 100 % B_{PE} is achieved with F:A 1 : 1 and 1 : 3 for *S. obliquus* with a culture of $OD_{680} \approx 2$. Since lesser input of fungal biomass in 1 : 3 F:A ratio gave similar output (99 % B_{PE}), hence, 1 : 3 F:A ratio was used in the rest of the experiments. Interestingly, previous reports also indicated that 1 : 3 F:A was the optimal ratio for harvesting of >95 % microalgal cells using the various filamentous fungi [20]. For example, Bhattacharya et al. [21] reported that *A. fumigatus* effectively bio-flocculates *C. pyrenoidosa* (B_{FE}> 95 %) at F:A ratio of 1 : 3. Likewise, *A. lentulus* FJ172995 completely bio-flocculates *Chroococcus* sp. within 6 h at 1 : 3 F:A ratio [20]. Overall, it is evident from the literature and present results that the 1 : 3 F:A ratio is the optimal ratio for harvesting *S. obliquus*.

3.2. Possible underlying mechanisms of microalgal-fungal pellets formation

To understand the possible mechanism of microalgal–fungal interaction, the surface properties of both fungus and microalgae were examined. Following the cultivation of *S. obliquus*, the pH of the culture medium was alkaline (pH ≈ 9.5) due to the formation of hydroxide ions during the photocatalytic conversion of light energy into oxygen in photosynthesis [2]. This alkaline pH leads to negative changes on the surface of microalgae. For further understanding, the electrokinetic charge and charge potential on the surface of microalgal cells were examined using zeta potential. The results revealed that *S. obliquus* exhibited a high zeta potential value of −3.7 mV at alkaline pH. This observation confirms the negative charge on the surface of *S. obliquus*, indicating a stable suspension at physiological pH. Apart from this, the net negative charge on the surface microalgae is due to carboxylic (– COOH), amine (– NH_2), and phosphate (– PO_4) groups [21]. FTIR analysis of the microalgal (*S. obliquus*) surface showed the presence of O – H group at 3425 cm^{-1}, possibly due to the presence of water or proteins (Fig. 2) [35]. Likewise, C = O of protein and P– O of phosphodiester group observed at 1650 cm^{-1} and 1242 cm^{-1} wavenumber, respectively [36,37]. The peak at 2926 cm^{-1} and 1727 cm^{-1} correspond to the stretching of aliphatic C–H and O–H groups, respectively [38,39]. Lastly, the peak at 1664, 1546, 1543, 1255, and 1242 cm^{-1} was mainly due to the presence of amide groups [35]. Furthermore, the pH of the fungus culture after cultivation was highly acidic (pH ≈ 4.85). The lower pH is primarily due to the production of organic acids such as citric acid or oxalic acid as metabolic by-products during fungal growth and reproduction [40]. Likewise, during respiration, fungi actively excrete hydrogen ions (protons) into the surrounding medium, leading to increased acidity. FTIR analysis of *A. fumigatus* revealed the presence of aromatic (C – C) stretch, aliphatic amines (C – N), primary amines (N – H), carboxylic (– COOH), and phosphate (– PO_4) groups at 1400 cm^{-1}, 1024 cm^{-1}, 1650 cm− [1], 3280 cm^{-1}, and 1250 cm− [1], respectively. However, these functional groups exist in a protonated form due to the highly acidic pH of the fungal culture.

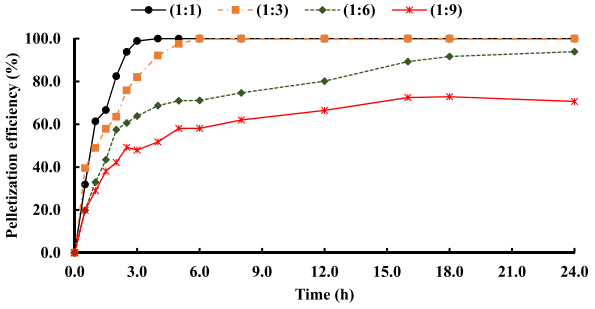

Fig. 1. Impact of different F:A ratios on microalgal biomass pelletization at elapsed time.

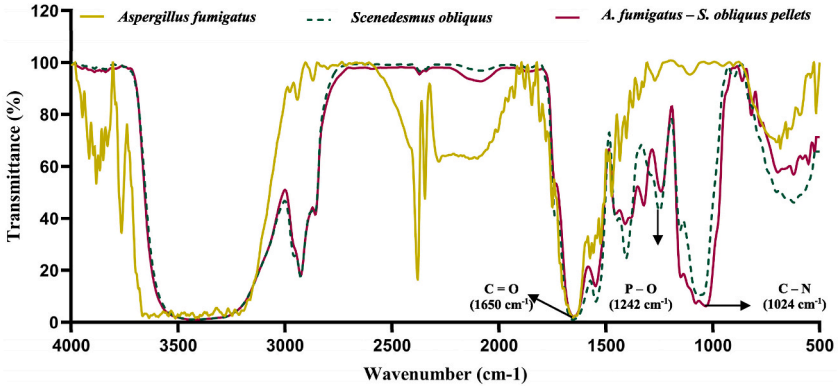

Fig. 2. Fourier transform infrared spectroscopy (FTIR) analysis of microalgae, fungus, and microalgal-fungal pellets (MAFP).

Consequently, a net positive charge is imparted on the fungal hyphae. Upon introduction of the fungus, a gradual decline in pH was observed, primarily attributed to the surplus positive charges on fungal hyphae. This pH reduction continues as microalgal cells progressively adhere to the fungal hyphae. After complete pelletization of microalgal cells, the resulting pH of the broth was nearly neutral (pH ≈ 6.92).

FTIR analysis of MAFP revealed significant variations in peak intensity at specific wavenumbers. Notably, the peak intensity (% transmittance) at 1242 cm^{-1} (P – O) exhibited a remarkable difference between microalgae (42.9 %) and MAFP (50.52 %). Likewise, at 1024 cm^{-1} (C – N), the peak intensity of fungal culture and MAFP were 99.6 %, and 6.16 %, respectively. However, in certain regions, the transmittance remained unchanged or slightly changed. For instance, at 1650 cm^{-1} (C = O), the transmittance values for microalgae, fungus, and MAFP were nearly identical, hovering around 3 %. These alterations in transmittance intensity imply the participation of these functional groups in microalgal-fungal interactions and characterize it as a physical biosorption process. Beyond surface interactions, some previous literature has suggested the potential involvement of metabolically active fungal biomass during pelletization [20]. For further understanding, an analysis of the Extracellular Polymeric Substances (EPS) in both microalgae and fungi before and after pelletization was estimated. It was observed that there was an increase in EPS production during MAFP formation, indicating metabolic fungi involvement in pelletization. Likewise, Prajapati et al. [20] observed that autoclaved fungal biomass was not capable of pelletization of microalgae. Therefore, it could be posited that fungal-mediated microalgal harvesting is not solely a physical process but encompasses both surface properties and fungal metabolic activity.

3.3. Physical and mechanical properties of microalgal-fungal pellets

The Visual and physical examination of all MAFP revealed spherical or oval masses intertwined hyphae in shape with an average diameter of 2.8 mm (Fig. 3). Besides, the sphericity of MAFP varied from pellet to pellet. Sphericity is a spherical or geometrical property of pellets that describes the degree to which pellets approach the shape of a perfect sphere. The sphericity of pellets ranges from 0 (non-spherical) to 1 (perfectly spherical). For instance, the sphericity of M_1 MAFP was observed to be 1 *i,e* perfectively spherical (Table 1). However, M_3, M_4, and M_5 microalgal pellets are spherical or near to perfectly spherical with sphericity around 0.92, 0.93,

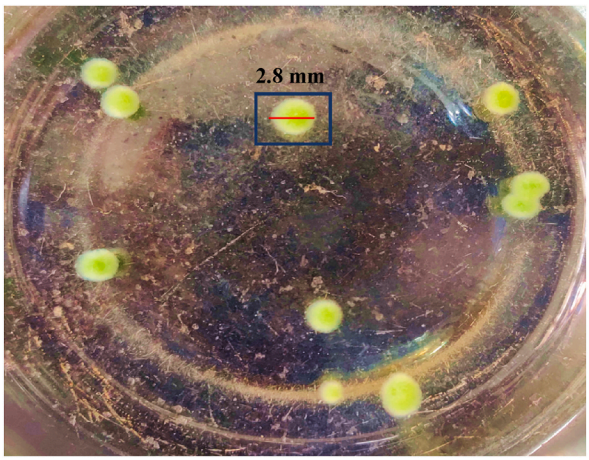

Fig. 3. Pictorial view of microalgae fungal pellets (MAFP) using a stereomicroscope.

and 0.89, respectively. The change in sphericity of MAFP is mainly due to slight variations in cell mass, which might be inherent in nature [41]. For example, in the logarithmic phase of microbial growth, cells generally exhibit a uniform division and exponential cell mass. However, it is crucial to acknowledge that some degree of variability in cell mass during microbial growth persists due to disparities in intracellular components (DNA, RNA, and proteins) [42].

Fig. 4 presented the Scanning Electron Microscopic (SEM) of *S. obliquus*, and *S. obliquus- A. fumigatus* pellets at 25.00 KX. From the results, it was observed that *S. obliquus* had a smooth and ellipsoidal outer surface, which is indicative of its characteristic morphology. In contrast, *A. fumigatus* exhibited a distinct elongated fibrous outer layer, highlighting the structural differences between the two organisms. A wall-to-wall fungal-microalgal interface between the two species was observed (Fig. 4 b). In addition, the SEM image revealed that the fungal hyphal network was physically contacted with small fibrous extensions of live microalgal cells [43]. The microalgal cells are ensnared within the fungal hyphal networks in the MAFP [44]. The fibrous extensions appeared to contribute to the attachment of the microalgae to hyphae, and irregular tube-like extensions were formed between the two interacting cell types. It is well-documented that fungal growth in submerged culture results in the secretion of various metabolites, including organic acids, polysaccharides, proteins, and enzymes. Therefore, the interaction and attachment of microalgal cells to fungal spores and hyphal surfaces may be mediated by these growth-associated metabolites secreted by the fungi [45]. After SEM analysis, the Energy Dispersive X-ray Spectroscopy (EDX) was used to quantify the elemental analysis of samples. Fig. 5 illustrates the variation in elemental analysis before and after microalgal pelletization. The data reveals that the carbon and nitrogen content in the microalgae was 62.9 $\pm$ 4.3 wt % and 14.1 $\pm$ 5.4 wt %, respectively (Fig. 5 a). However, after pelletization, the carbon and nitrogen content reduced to 54.4 $\pm$ 2.4 wt % and 9.0 $\pm$ 3.6 wt %, respectively (Fig. 5 b). In contrast, the oxygen content after pelletization increased to 36.6 $\pm$ 2.2 wt % from 22.9 $\pm$ 2.4 wt % (microalgae). This shift in elemental content may be attributed to the breakdown or transformation of organic carbon-containing compounds. For instance, during microalgal-fungal pelletization, species often produce extracellular polymeric substances (EPS), which contribute to the structure and cohesion of the pellets [45]. These EPS might contain lower carbon content than the microalgae cells, affecting the overall biomass carbon content. Additionally, the lower protein content in microalgal pellets (56.25 wt %) compared to microalgae (88.12 wt %) further corroborates the EPS production and alterations in elemental composition.

The mechanical properties, including the density and detachment rate of MAFP, play a crucial role in the immobilization of microalgae to fungal pellets. For example, optimal density ensures a stable structure, preventing detachment of microalgae and enhanced mass transfer. Likewise, the detachment rate prevents the premature release of microalgae, maintaining long-term stability. From the data, it was observed that the density of a single MAFP was extremely low, *i.e.,* 0.044 kg/m^3. The lower density indicates that MAFP has a porous or loosely packed structure. A porous or permeable structure can facilitate the diffusion of nutrients and gases within the pellet, allowing for the efficient exchange of substances between the pellet interior and the surrounding environment. Moreover, a porous structure provides a larger surface area, leading to enhanced contact between microalgae and the effluent, potentially improving system efficiency. A loosely packed structure may be more resilient to shear forces, as evidenced by the zero-detachment rate observed after 9 days of incubation at 120 rpm. A thorough review of the existing literature revealed no prior studies explicitly evaluating the mechanical properties of MAFP. However, a study by Wang et al. [46] reported a density of 40.37 kg/m^3 for algae-fungal consortia, which significantly exceeds the density observed in present investigation.

3.4. Pollutant removal assessment by microalgal-fungal pellets

The changes in pollutant concentration at varying time intervals are depicted in Fig. 6. From the results, it was observed that MAFP effectively and rapidly uptakes nutrients (NH_3-N, NO_3^--N, and PO_4^{3-}) from HE without any lag phase or latent phase. It might be due to MAFP already being in their exponential phase or previously adapted to operational conditions such as light intensity, temperature, and mixing rate [2,5,47]. However, the response of MAFP to NH_3-N, NO_3^--N, and PO_4^{3-} uptake efficiency exhibited differential patterns. For example, during the first two days of the MAFP incubation, the NH_3-N, and PO_4^{3-} concentrations exhibited rapid declines with uptake efficiencies 44.00 % and 39.96 %, respectively. At the same time, the NO_3^-–N uptake efficiency was slightly low (11.03 %). In addition, within 7 days, MAFPs completely (100 %) assimilate NH_3-N and PO_4^{3-} from HE. Besides, >80 % NO_3^--N removal was observed within 7 days, with complete removal on 9th day. On the other hand, fungal pellets did not show complete nutrient removal from the HE. However, only a small amount of nutrient uptake by the fungal pellets was observed. From the results, it was noted that >50 % of PO_4^{3-} and 20 % of NH_3-N were uptake by fungal pellets within 9 days. Additionally, NO_3^--N removal by fungal pellets was extremely poor, with an 8.09 % uptake efficiency. The higher PO_4^{3-}, and of NH_3-N uptake by fungal pellets might be due to the fact that fungus readily utilized nitrogen in the form of NH_4^+, and phosphate in any form for their growth and cellular processes [48]. Moreover, our previous findings suggest that *S obliquus* rapidly thrives and uptakes nutrients efficiently. However, the time required for complete mineralization was relatively longer (15–16 d) than MAFP (7–9 d). Therefore, MAFP presents a more advantageous option for nutrient

Table 1
Physical properties of microalgal-fungal pellets.

Microalgal-fungal pellets (MAFP)	Shortest diameter (mm)	Longest diameter (mm)	Average diameter (mm)	Sphericity
M_1	3.0	3.0	3.0	1.00
M_2	2.5	2.9	2.7	0.80
M_3	2.6	2.8	2.7	0.92
M_4	2.8	3.0	2.9	0.93
M_5	2.5	2.8	2.6	0.89

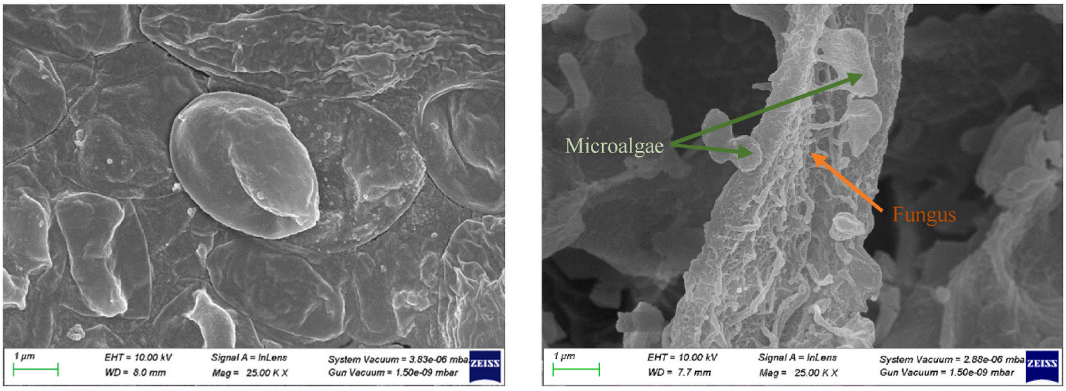

Fig. 4. FESEM analysis of (a) Microalgae and (b) Microalgal-fungal pellets (MAFP).

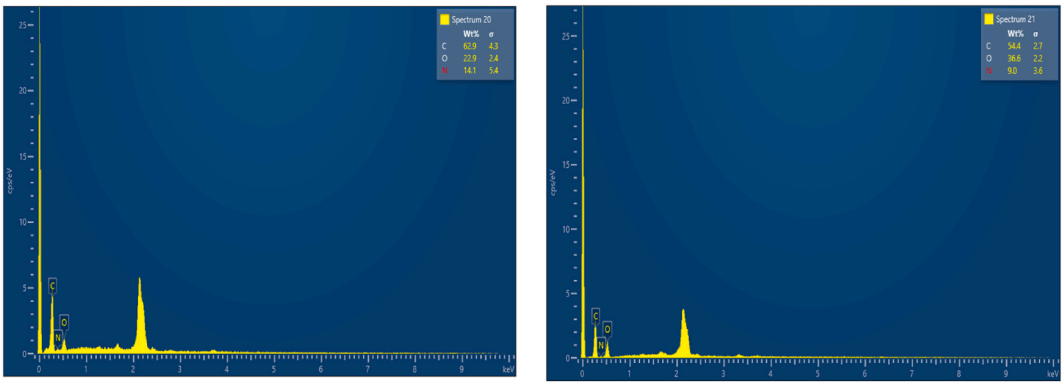

Fig. 5. EDX of (a) Microalgae and (b) Microalgal-fungal pellets (MAFP).

recovery and rapid biomass harvesting.

Fig. 7 illustrates the pollutant uptake rate (P_r) by MAFP and fungal pellets at varying time intervals. Surprisingly, NH_3-N, and PO_4^{3-} exhibited significantly higher P_r throughout the experiment when compared with NO_3^--N for both MAFP and fungal pellets. However, it is interesting to note that the NH_3-N, NO_3^--N, and PO_4^{3-} uptake rate of MAFP was relatively higher than the fungal pellets. The NH_3-N, and PO_4^{3-} uptake rate presented the asymmetrical bell-shaped curve, with the highest P_r was observed to be 5.50 ± 0.1 mg $L^{-1}d^{-1}$ and 8.62 ± 0.12 mg $L^{-1}d^{-1}$, respectively, on 2nd day of the MAFP growth. Besides, NO_3^--N represented the logarithmic uptake rate curve with the highest P_r was observed to be 3.24 ± 0.6 mg $L^{-1}d^{-1}$, on 7th day of the MAFP growth. In contrast, fungal pellets showed different uptake profiles for NH_3-N, NO_3^--N, and PO_4^{3-}. For instance, NH_3-N, uptake rate presented the asymmetrical bell-shaped curve with highest P_r was observed to be 0.84 ± 0.1 mg $L^{-1}d^{-1}$, on 5th day. Besides, PO_4^{3-} represented the logarithmic uptake rate curve with the log phase was observed from 0 – 5th day of the fungal pellets incubation. On the other hand, a completely different NO_3^--N, uptake rate profile was observed for fungal pellets. Until the 5th day of fungal pellets incubation, negligible or no NO_3^--N uptake was observed. However, 5th day onwards, a slight increase in NO_3^--N uptake was observed, reaching the highest P_r of 0.24 ± 0.07 mg $L^{-1}d^{-1}$ on the 9th day of fungal pellet incubation. Consistent with the observed trends, the average specific pollutant uptake rate (μ_r) further strengthened the first preferential uptake of NH_3-N, and PO_4^3 for both MAFP and fungal pellets (Table 2). For example, the average NH_3-N, and PO_4^3 μ_r for MAFP was 0.143 ± 0.01 d^{-1}, and 0.131 d^{-1}, respectively. Whereas, in the case of NO_3^--N, the average μ_r was relatively poor at 0.08 d^{-1}, highlighting the disparity in uptake efficiency across various nutrient types. These differences in nutrient uptake efficiency might be due to two possible reasons. (i) Luxury uptake of phosphorus from phosphorus abundance environment [49]. Under the luxury phosphate uptake mechanism, microalgae store phosphate as Acid Insoluble Polyphosphate (ASAP) in the vacuole within one to 2 h for further division of cells up to several generations without any other external sources [49–53]. (ii) Conversion of nitrate, nitrite to ammonium ion during nitrogen assimilation pathways. For microalgae, ammonium (NH_4^+) ions are most preferable among inorganic nitrogen sources due to less energetic demands and fewer genes involved in metabolism. However, for NO_3^- and NO_2^-, their assimilation into the GS/GOGAT pathways requires a stepwise reduction to NH_4^+ using nitrate reductase (NR) and nitrite reductase (N_iR) enzymes. Besides, these reductase enzymes require NADH (NR) and ferredoxin (NiR) as electron donors to conduct the reduction process [54]. This energy-dependent pathway likely underlies the observed lower nitrate uptake relative to phosphate and ammonia during growth.

Beyond NH_3-N, NO_3^--N, and PO_4^{3-}, HE also contains dissolved solids (≈0.53 g/L) in the form of hydrogen carbonate ions, sodium,

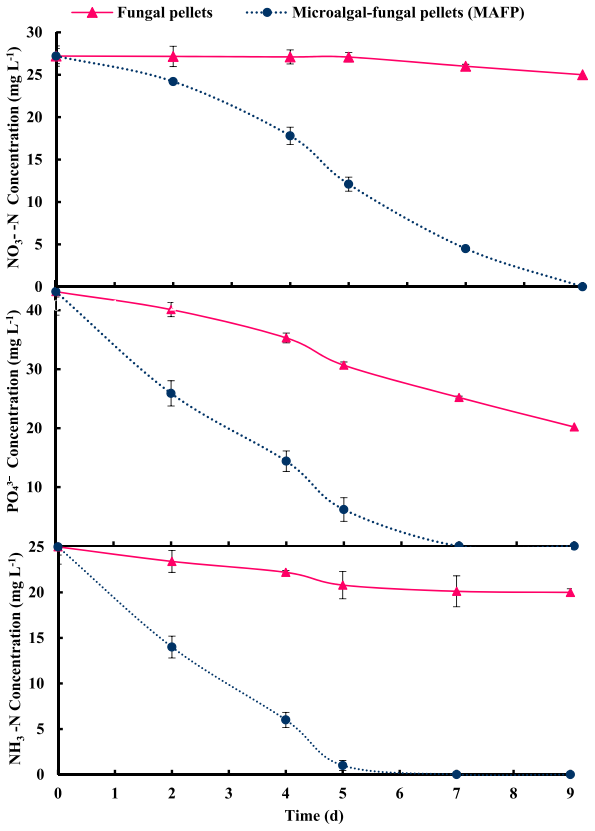

Fig. 6. Pollutant removal potential of Microalgal-fungal pellets (MAFP), and Fungal pellets at varying time intervals.

potassium, chloride, calcium, and magnesium salts [5,55]. However, these dissolved solids were found to be within the Indian water discharge limit standards (2.1 g/L). To understand whether the resulting levels remain within permissible limits or if there are potential exceedances, dissolved solids, salinity, and conductivity of the treated water after MAFP cultivation were analyzed. The results showed that the total dissolved solid after treatment decreased *i,e* 0.23 g/L. Likewise, the salinity and the conductivity were reduced (0.4 g/kg, and 713 mS/cm, respectively). Previous studies also suggested that microalgae are capable of removing dissolved solids from wastewater. For instance, Peng et al. [56] demonstrated the effectiveness of an algal biofilm reactor in treating synthetic industrial effluent with high dissolved solids. Their findings revealed a significant reduction in total dissolved solids, achieving removal rates of 2783 mg L^{-1}-d^{-1} and 19,530 mg m^{-2} d^{-1}. The decrease in dissolved solids might be attributed to the intake of salts and ions by microalgae during their cellular metabolism. For example, during NO_3^- uptake mechanism, the co-transport system is typically energized by a proton ($2H^+$) or sodium ($2Na^+$) gradient [57]. Moreover, chloride (Cl^-) participates in the co-transport of NO_3^- and NO_2^- under high CO_2 conditions [58]. However, it is important to note that certain ions, such as K^+, and Li^+, may also inhibit these transport systems [59]. In addition, Upon nine days of incubation in HE, the final biomass concentration of MAFP was observed to be 2.7 ± 0.36 g/L. Besides, the final biomass concentration of HE-grown microalgae and fungal pellets were 1.42 ± 0.12 g/L and 0.5 g/L ± 0.04, respectively. The biomass productivity of fungal pellets and microalgae in HE were 8.42 ± 1.1 mg L^{-1} d^{-1}, and 138.93 ± 4.11 mg L^{-1} d^{-1}, respectively. Whereas, with MAFP in HE treatment, remarkably higher biomass production (567.12 ± 1.7 mg L^{-1} d^{-1}) was recorded. Overall, it is evident from the present finding that MAFP could thrive in HE with improved biomass productivity and nutrient uptake capabilities, positioning it as a promising technology for sustainable wastewater treatment and resource recovery.

3.5. *Biochemical and elemental analysis of microalgal-fungal pellets*

For any living creature, biomolecules such as lipids, carbohydrates, and proteins are the essential components for their growth, cellular function, and survival. These biomolecules contribute to diverse biological processes. For example, carbohydrates and lipids serve as primary energy sources for cellular metabolism and providing precursors for cell membrane biosynthesis. Proteins, on the other hand, contribute to the structural integrity and cellular signaling of the cells. Further, it is evident that the concentration of biomolecules within microalgal cells varies and might be influenced by the nutrient composition of the growth media and surface-attached microorganisms. A comparison of biochemical composition (% TS) between MAFP, fungal pellets, and microalgae is shown in Fig. 8 (a). The biochemical composition and the elemental analysis of microalgal biomass were taken from our previous results [2]. MAFP showed the highest protein content, 52.06 ± 2.1 % TS, among all the tested biomass (microalgae and fungal pellets).

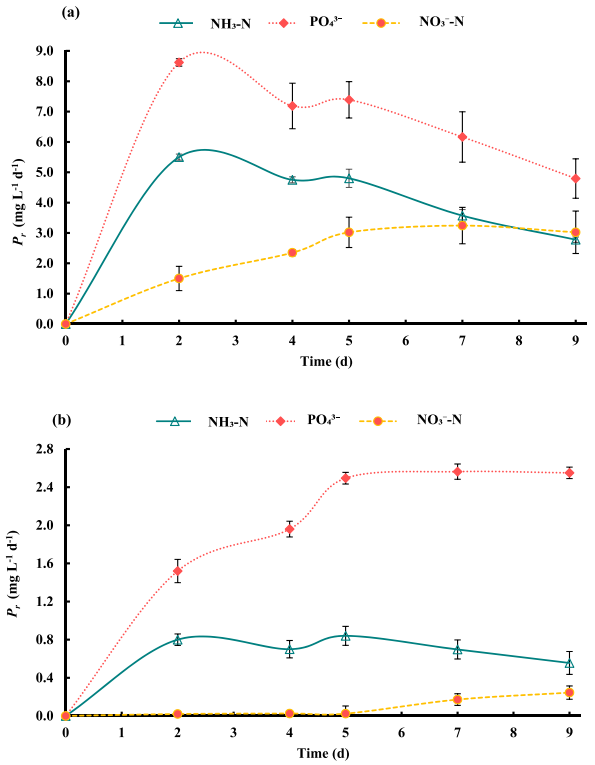

Fig. 7. Pollutant uptake rate of (a) Microalgal-fungal pellets (MAFP), (b) Fungal pellets at varying time intervals.

Table 2
Specific pollutant uptake rate of microalgal-fungal pellets (MAFP) and fungal pellets.

Time (d)	Specific pollutant uptake rate (d^{-1})					
	NH_3 -N		PO_4^{3-}		NO_3^- -N	
	MAFP	Fungal pellets	MAFP	Fungal pellets	MAFP	Fungal pellets
1	0.22 ± 0.01	0.032 ± 0.001	0.20 ± 0.12	0.035 ± 0.002	0.05 ± 0.00	0.000 ± 0.000
3	0.19 ± 0.01	0.028 ± 0.011	0.16 ± 0.08	0.045 ± 0.008	0.08 ± 0.01	0.000 ± 0.000
5	0.19 ± 0.03	0.034 ± 0.003	0.17 ± 0.06	0.058 ± 0.006	0.12 ± 0.08	0.000 ± 0.000
7	0.14 ± 0.01	0.028 ± 0.002	0.14 ± 0.08	0.059 ± 0.008	0.11 ± 0.06	0.006 ± 0.000
9	0.11 ± 0.04	0.022 ± 0.004	0.11 ± 0.06	0.059 ± 0.001	0.11 ± 0.07	0.009 ± 0.000

Besides, microalgae and fungal pellets had a 50.13 ± 1.00 % TS, and 34 ± 1.7 % TS, of protein. The observed higher protein content might be attributed to two potential reasons: (i) High nitrogen and phosphorus concentration in HE, impacting protein biosynthesis [60]. Generally, nitrogen assimilation in microalgae occurs via glutamine synthetase and glutamate synthase pathways [61–63]. Once nitrogen is assimilated into glutamate and glutamine, the aminotransferases distribute amino acids, which serve as building blocks for protein synthesis. Excess nitrogen results in the overproduction of amino acids, while insufficient nitrogen decreases cellular protein levels and the potential recycling of nitrogen into amino acids to mitigate stress. Likewise, higher phosphate levels in the growth media could be attributed to a higher protein content because phosphorus is a key component of ATP (adenosine triphosphate). Excess phosphorus leads to increased ATP production, ultimately resulting in the production of more amino acids [2,49].

$$TP + (Phosphate)_n \rightleftarrows ADP + (Phosphate)_{n+1}$$

(ii) Potential induction of protein synthesis in microalgae as stress response during pelletization, potentially linked to the production of exopolysaccharides (EPS) as a defense mechanism against fungal predation [64].

Furthermore, the carbohydrates and lipid content of microalgal biomass was observed to be 10.05 ± 0.09 % TS, and 36.67 ± 1.90 % TS, respectively. Whereas, in the case of MAFP biomass, the carbohydrate content increased to 28.95 ± 0.05 % TS, and the lipid content decreased to 18.36 ± 0.12 % TS. The observed variation in carbohydrate and lipid accumulation within MAFPs might be attributed to the upregulation of starch metabolic pathways in the microalgae. Previous literature suggests that following interaction

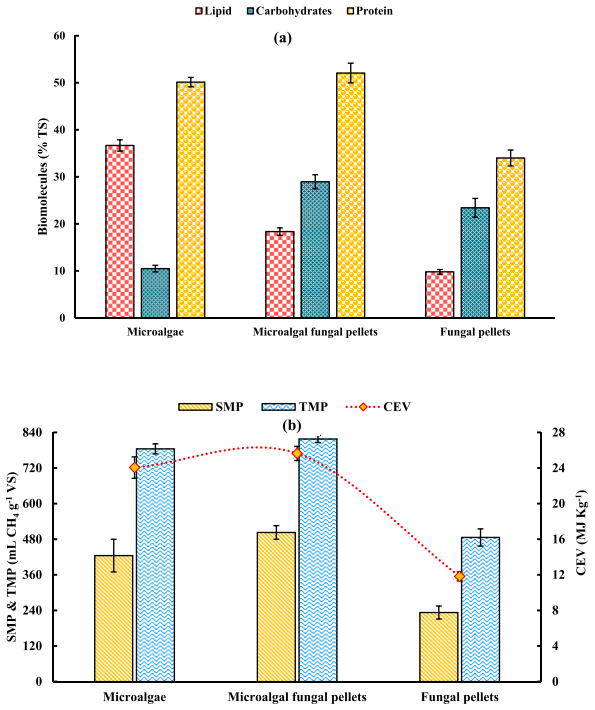

Fig. 8. Comparison of (a) Biochemical composition and (b) Methane potential yield of microalgal-fungal pellets (MAFP), microalgae, and fungal pellets.

with fungi, microalgae exhibit significant upregulation of diverse metabolic pathways, such as carbohydrate metabolism glycolysis/gluconeogenesis, pyruvate metabolism, amino acids biosynthesis, nucleotide sugar, amino sugar, purine metabolism, oxidative phosphorylation, and glutathione metabolisms were significantly up-regulated in the microalgae [65]. Remarkably, genes encoding glycolytic key enzymes such as pyruvate kinase (*pyk 1)*, and phosphofructokinase (*pfk1)* were significantly upregulated, catalyze the conversion of phosphoenolpyruvate to pyruvate and phosphorylation of fructose-6-phosphate, respectively [66]. Subsequently, pyruvate enters into the TCA cycle where pyruvate dehydrogenase complex/carrier (*pda1*) and citrate synthase (*cts1*) get upregulated the acetyl-Co-A, and biosynthesis of amino acids [67]. A recent study conducted by Li et al. [68] where *Chlorella pyrenoidosa*, and *Debaryomyces hansenii* were co-cultivated in synthetic wastewater. The results revealed a significant increase in carbohydrate (24.2 ± 4.2 % TS) content in the co-culture compared to the microalgae culture (19.4 ± 2.7 % TS). Overall, it can be concluded that MAFP generates more carbohydrates than lipids. However, the protein content of MAFP was remarkably higher. It is evident from the literature that *S. obliquus* contains high protein content (50–56 % TS) and is used as a food protein or dietary supplement such as Chlorophyceae [69]. Moreover, *S. obliquus* protein is used as a sustainable emulsifier for the food industries [70]. Microalgae-based proteins offer various health benefits such as anti-hypertension, anti-hyperlipidemia, renal protection, and anti-hyperglycaemic [71]. For example, *Spirulina* proteins have high levels of γ-linoleic acid, B vitamins, and free-radical scavenging phycobiliproteins [72]. Apart from this, two bioactive proteins such as Lectins and phycobiliproteins, have been strategically utilized for several industrial applications. Lectins a well-known glycoproteins used by various biotechnological industries as cancer biomarkers, blood grouping, cell-cell communication, Likewise, phycobiliproteins are used in fluorescent labelling, flow cytometry, fluorescent microscopy, and fluorescent immunohistochemistry [73,74].

The elemental composition of MAFP, microalgae, and microalgal biomass is presented in Table 3. The carbon content of MAFP and microalgae was 59.41 ± 0.13 % TS, and 50.44 ± 0.28 % TS, respectively. Besides, the carbon content of fungal pellets was relatively low *i,e* 25.69 ± 0.15 % TS. Similarly, the nitrogen content in MAFP (8.33 ± 0.05 % TS), and microalgae (8.02 ± 0.08 % TS) were also higher than fungal pellets biomass (5.44 ± 0.08 % TS). The observed higher nitrogen content in microalgae and MAFP is likely attributable to their efficient uptake of nitrogen from HE. In contrast, the hydrogen content of MAFP (5.89 ± 0.03 % TS) was lower compared to microalgae (7.53 ± 0.12 % TS). The decrease in hydrogen content in MAFP can be attributed to differing metabolic processes and composition between microalgae and fungal biomass. Fungal pellets typically have lower hydrogen content (4.21 ± 0.06 % TS), which reduces the overall hydrogen content when integrated with microalgae. The carbon to nitrogen (C/N) ratios of fungal and microalgal biomass were observed to be 4.72 ± 0.09 % TS, and 6.29 ± 0.12 % TS, respectively. Notably, upon the combination of microalgae to fungal biomass, the C/N ratio (7.13 ± 0.03 % TS) was increased. Furthermore, the estimated CEV, SMP, and TMP of the tested biomass are shown in Fig. 8 (b). From the results it was well obvious that the CEV potential of MAFP (25.63 ± 0.03 MJ kg^{-1}) was the highest among microalgae (24.05 ± 1.2 MJ kg^{-1}), and fungal pellets biomass (11.82 ± 0.5 MJ kg^{-1}). As expected from the biomass composition, significant differences in the SMP and TMP were observed among the tested biomass. The observed differences in SMP and TMP values might be attributed to their distinct estimation methodologies. TMP is estimated based on the total elemental

Table 3
Elemental composition of microalgal-fungal pellets (MAFP), microalgae, and fungal pellets.

Biomass	Carbon (% TS)	Nitrogen (% TS)	Hydrogen (% TS)	Sulfur (% TS)	C/N ratio	C/H ratio	Empirical formula
Microalgae	50.44 ± 0.28	8.02 ± 0.08	7.53 ± 0.12	0.65 ± 0.42	6.29 ± 0.12	6.70 ± 0.10	$C_{206}H_{368}N_{28}O_{102}S$
Microalgal-fungal pellets (MAFP)	59.41 ± 0.13	8.33 ± 0.05	5.89 ± 0.03	1.23 ± 0.18	7.13 ± 0.03	10.09 ± 0.09	$C_{33}H_{38}N_4O_{10}S$
Fungal pellets	25.69 ± 0.15	5.44 ± 0.08	4.21 ± 0.06	2.17 ± 0.12	4.72 ± 0.09	6.09 ± 0.21	$C_{31}H_{61}N_5O_{57}S$

composition (% TS) of the biomass. However, SMP emphasizes easily degradable biomolecules such as lipids, carbohydrates, and proteins known to have high methane production potential. The calculated SMP, and TMP values for MAFP were 502.74 ± 19.1 mL CH_4 g^{-1} VS, and 817.68 ± 12.5 mL CH_4 g^{-1} VS, respectively. Besides, calculated SMP and TMP for microalgal biomass were 424.73 ± 55.2 mL CH_4 g^{-1} VS, and 784.47 ± 17.3 mL CH_4 g^{-1} VS. Conversely, the maximum possible methane potential for fungal pellets biomass was extremely lower (TMP ≈ 485.88 ± 29 mL CH_4 g^{-1} VS, and SMP ≈ 232.77 ± 22.4 mL CH_4 g^{-1} VS). From the results, it could be postulated that anaerobic co-digestion of microalgae with fungal biomass results in enhanced biomethane yield. The improved biomethane yield in MAFP might be attributed to the role of the fungus in the pretreatment of microalgal biomass. Further, Prajapati et al. [20] also demonstrated that during the incubation of MAFP, a significant production of cellulase enzyme by the fungus leads to the release of soluble sugars from microalgal cells. Consequently, there was a >54 % enhancement in digestibility and a marked increase (up to 50 %) in biomethane production from MAFP during anaerobic digestion [20]. Hence, it can be concluded that there is significant potential of MAFP in biomethane production, making it a promising feedstock for bioenergy and the production of value-added products.

4. Conclusions

The present study demonstrated that MAFP can photosynthetically bio-convert HE into biochemical-rich biomass. Testing various F:A ratios revealed 100 % microalgal biomass harvesting efficiency at 1:3 within 6 h. Interaction studies revealed that metabolically active fungi with opposite charges facilitate microalgal pelletization. The physical and mechanical properties suggest that the porous structure of MAFP enables efficient nutrient uptake. Further, the findings reveal that MAFP could thrive in HE by effectively utilizing nutrients within a short time frame. The produced biomass was enriched with high levels of metabolites (lipids, proteins, and carbohydrates), indicating its suitability for biomethane production. In essence, the present findings suggest that MAFP can be an effective and sustainable solution for HE treatment, with the produced biochemically rich biomass serving as an excellent feedstock for bioenergy production. However, further pilot scale to commercial scale validation is warranted to assess its feasibility for real-world applications.

Data availability

Data will be made available on request.

CRediT authorship contribution statement

Harshit Tiwari: Writing – original draft, Methodology, Conceptualization. **Sanjeev Kumar Prajapati:** Writing – review & editing, Funding acquisition, Conceptualization.

Declaration of competing interest

The authors declare that they have no known competing financial interests or personal relationships that could have appeared to influence the work reported in this paper.

Acknowledgments

The authors are thankful to the Science and Engineering Research Board (SERB), Govt. of India for providing financial support for the present work through Core Research Grant (CRG) scheme (Grant No. CRG/2021/005018). Moreover, Harshit Tiwari is thankful to Ministry of Education (MoE), Govt. of India, for providing the Prime Minister's Research Fellowship (PMRF ID-2802484). Mr. Satyapal Singh and Ms. Sudha are acknowledged for the laboratory assistance. The authors are grateful to the Institute Instrumentation Centre (IIC), and Central Instrumentation Facility, Department of Chemical Engineering, Indian Institute of Technology Roorkee for providing various instruments for the research work.

References

[1] Camille Boylan, The Future of farming: hydroponics. https://psci.princeton.edu/tips/2020/11/9/the-future-of-farming-hydroponics, 2020.
[2] H. Tiwari, S.K. Prajapati, Photosynthetic bioconversion of hydroponic effluent into biochemical-rich biomass for microalgal biorefineries, Environ. Sci. Water Res. Technol. 9 (2023) 2692–2705, https://doi.org/10.1039/d3ew00327b.
[3] H. Tiwari, S.K. Prajapati, Hydroponics effluent recycling for bioenergy using microalgae, in: B.-M. Hodge, S.K. Prajapati (Eds.), Lecture Notes in Civil Engineering, Springer Nature Singapore, 2024, pp. 319–325, https://doi.org/10.1007/978-981-99-6616-5_36.
[4] M. Majid, J.N. Khan, Q.M. Ahmad Shah, K.Z. Masoodi, B. Afroza, S. Parvaze, Evaluation of hydroponic systems for the cultivation of Lettuce (Lactuca sativa L., var. Longifolia) and comparison with protected soil-based cultivation, Agric. Water Manag. 245 (2021) 106572, https://doi.org/10.1016/j.agwat.2020.106572.
[5] H. Tiwari, S.K. Prajapati, Allelopathic effect of benzoic acid (hydroponics root exudate) on microalgae growth, Environ. Res. 219 (2023) 113260, https://doi.org/10.1016/j.envres.2022.115020.
[6] P. Saxena, A. Bassi, Removal of nutrients from hydroponic greenhouse effluent by alkali precipitation and algae cultivation method, J. Chem. Technol. Biotechnol. 88 (2013) 858–863, https://doi.org/10.1002/jctb.3912.
[7] A. Richa, S. Touil, M. Fizir, V. Martinez, Recent advances and perspectives in the treatment of hydroponic wastewater: a review, Rev. Environ. Sci. Biotechnol. 19 (2020) 945–966, https://doi.org/10.1007/s11157-020-09555-9.
[8] J.M. O'Neil, T.W. Davis, M.A. Burford, C.J. Gobler, The rise of harmful cyanobacteria blooms: the potential roles of eutrophication and climate change, Harmful Algae 14 (2012) 313–334, https://doi.org/10.1016/j.hal.2011.10.027.
[9] B.-S. Choi, S.-S. Lee, Y.M. Awad, Y.-S. Ok, Feasibility of Reclaimed wastewater and waste nutrient solution for crop production in Korea, Korean J. Environ. Agric. 30 (2011) 118–124, https://doi.org/10.5338/kjea.2011.30.2.118.
[10] S. Koide, N. Satta, Separation performance of ion-exchange membranes for Electrolytes in drainage nutrient solutions subjected to Electrodialysis, Biosyst. Eng. 87 (2004) 89–97, https://doi.org/10.1016/j.biosystemseng.2003.09.005.
[11] J.H. Park, S.H. Kim, R.D. Delaune, J.S. Cho, J.S. Heo, Y.S. Ok, D.C. Seo, Enhancement of nitrate removal in constructed wetlands utilizing a combined autotrophic and heterotrophic denitrification technology for treating hydroponic wastewater containing high nitrate and low organic carbon concentrations, Agric. Water Manag. 162 (2015) 1–14, https://doi.org/10.1016/j.agwat.2015.08.001.
[12] J.A.C. Castellar, J. Formosa, A.I. Fernández, P. Jové, M.G. Bosch, J. Morató, H. Brix, C.A. Arias, Cork as a sustainable carbon source for nature-based solutions treating hydroponic wastewaters – Preliminary batch studies, Sci. Total Environ. 650 (2019) 267–276, https://doi.org/10.1016/j.scitotenv.2018.08.365.
[13] K.W. Chew, K.S. Khoo, H.T. Foo, S.R. Chia, R. Walvekar, S.S. Lim, Algae utilization and its role in the development of green cities, Chemosphere 268 (2021) 129322, https://doi.org/10.1016/j.chemosphere.2020.129322.
[14] W.N.A. Kadir, M.K. Lam, Y. Uemura, J.W. Lim, K.T. Lee, Harvesting and pre-treatment of microalgae cultivated in wastewater for biodiesel production: a review, Energy Convers. Manag. 171 (2018) 1416–1429, https://doi.org/10.1016/j.enconman.2018.06.074.
[15] G. Pankaj, T. Harshit, S. Priyanka, B. Bhunia, Role of biomass-based biorefinery in mitigating environmental pollution, in: Clean Technologies toward a Sustainable Future: Physicochemical, Biochemical and Biotechnological Approaches, 2023, pp. 1–342, https://doi.org/10.2166/9781789063783.
[16] A.I. Barros, A.L. Gonçalves, M. Simões, J.C.M. Pires, Harvesting techniques applied to microalgae: a review, Renew. Sustain. Energy Rev. 41 (2015) 1489–1500, https://doi.org/10.1016/j.rser.2014.09.037.
[17] F. Fasaei, J.H. Bitter, P.M. Slegers, A.J.B. van Boxtel, Techno-economic evaluation of microalgae harvesting and dewatering systems, Algal Res. 31 (2018) 347–362, https://doi.org/10.1016/j.algal.2017.11.038.
[18] S. Salim, R. Bosma, M.H. Vermuë, R.H. Wijffels, Harvesting of microalgae by bio-flocculation, J. Appl. Phycol. 23 (2011) 849–855, https://doi.org/10.1007/s10811-010-9591-x.
[19] D. Vandamme, I. Foubert, K. Muylaert, Flocculation as a low-cost method for harvesting microalgae for bulk biomass production, Trends Biotechnol. 31 (2013) 233–239, https://doi.org/10.1016/j.tibtech.2012.12.005.
[20] S.K. Prajapati, A. Bhattacharya, P. Kumar, A. Malik, V.K. Vijay, A method for simultaneous bioflocculation and pretreatment of algal biomass targeting improved methane production, Green Chem. 18 (2016) 5230–5238, https://doi.org/10.1039/c6gc01483f.
[21] A. Bhattacharya, M. Mathur, P. Kumar, S.K. Prajapati, A. Malik, A rapid method for fungal assisted algal flocculation: critical parameters & mechanism insights, Algal Res. 21 (2017) 42–51, https://doi.org/10.1016/j.algal.2016.10.022.
[22] C. Jeong, S. Kim, C. Lee, S. Cho, S.B. Kim, Changes in the physical properties of calcium alginate gel beads under a wide range of gelation temperature conditions, Foods 9 (2020) 180, https://doi.org/10.3390/foods9020180.
[23] J. Xue, Y. Wu, K. Shi, X. Xiao, Y. Gao, L. Li, Y. Qiao, Study on the degradation performance and kinetics of immobilized cells in straw-alginate beads in marine environment, Bioresour. Technol. 280 (2019) 88–94, https://doi.org/10.1016/j.biortech.2019.02.019.
[24] W. Zhou, Y. Cheng, Y. Li, Y. Wan, Y. Liu, X. Lin, R. Ruan, Novel fungal pelletization-assisted technology for algae harvesting and wastewater treatment, Appl. Biochem. Biotechnol. 167 (2012) 214–228, https://doi.org/10.1007/s12010-012-9667-y.
[25] S.A. Channiwala, P.P. Parikh, A unified correlation for estimating HHV of solid, liquid and gaseous fuels, Fuel 81 (2002) 1051–1063, https://doi.org/10.1016/S0016-2361(01)00131-4.
[26] G.E. Symons, A.M. Buswell, The methane Fermentation of carbohydrates, J. Am. Chem. Soc. 55 (1933) 2028–2036, https://doi.org/10.1021/ja01332a039.
[27] S.K. Prajapati, A. Malik, V.K. Vijay, Comparative evaluation of biomass production and bioenergy generation potential of Chlorella spp. through anaerobic digestion, Appl. Energy 114 (2014) 790–797, https://doi.org/10.1016/j.apenergy.2013.08.021.
[28] M. Bhandari, S.K. Prajapati, Use of reverse osmosis reject from drinking water plant for microalgal biomass production, Water Res. 210 (2022) 117989, https://doi.org/10.1016/j.watres.2021.117989.
[29] M.S. Rana, S.K. Prajapati, Microwave-assisted pretreatment of wet microalgal biomass for recovery of biofuel precursors, Fuel 305 (2021) 121610, https://doi.org/10.1016/j.fuel.2021.121610.
[30] M.S. Rana, S.K. Prajapati, Stimulating effects of glycerol on the growth, phycoremediation and biofuel potential of Chlorella pyrenoidosa cultivated in wastewater, Environ. Technol. Innov. 24 (2021) 102082, https://doi.org/10.1016/j.eti.2021.102082.
[31] M.S. Rana, S. Bhushan, D.R. Sudhakar, S.K. Prajapati, Effect of iron oxide nanoparticles on growth and biofuel potential of Chlorella spp, Algal Res. 49 (2020) 101942, https://doi.org/10.1016/j.algal.2020.101942.
[32] A.W.D. Larkum, I.L. Ross, O. Kruse, B. Hankamer, Selection, breeding and engineering of microalgae for bioenergy and biofuel production, Trends Biotechnol. 30 (2012) 198–205, https://doi.org/10.1016/j.tibtech.2011.11.003.
[33] Y. Fan, J. Wang, C. Gao, Y. Zhang, W. Du, A novel exopolysaccharide-producing and long-chain n-alkane degrading bacterium Bacillus licheniformis strain DM-1 with potential application for in-situ enhanced oil recovery, Sci. Rep. 10 (2020), https://doi.org/10.1038/s41598-020-65432-z.
[34] G. Ding, X. Li, W. Lin, Y. Kimochi, R. Sudo, Enhanced flocculation of two bioflocculation-producing bacteria by secretion of Philodina erythrophthalma, Water Res. 112 (2017) 208–216, https://doi.org/10.1016/j.watres.2017.01.044.
[35] N.E. El-Naggar, R.A. Hamouda, G.W. Abou-El-Souod, Statistical optimization for simultaneous removal of methyl red and production of fatty acid methyl esters using fresh alga Scenedesmus obliquus, Sci. Rep. 12 (2022) 7156, https://doi.org/10.1038/s41598-022-11069-z.
[36] J.N. Murdock, D.L. Wetzel, FT-IR microspectroscopy enhances biological and ecological analysis of algae, Appl. Spectrosc. Rev. 44 (2009) 335–361, https://doi.org/10.1080/05704920902907440.
[37] K. Stehfest, J. Toepel, C. Wilhelm, The application of micro-FTIR spectroscopy to analyze nutrient stress-related changes in biomass composition of phytoplankton algae, Plant Physiol. Biochem. 43 (2005) 717–726, https://doi.org/10.1016/j.plaphy.2005.07.001.
[38] R. Saha, K. Mukherjee, I. Saha, A. Ghosh, S.K. Ghosh, B. Saha, Removal of hexavalent chromium from water by adsorption on mosambi (Citrus limetta) peel, Res. Chem. Intermed. 39 (2013) 2245–2257, https://doi.org/10.1007/s11164-012-0754-z.
[39] S. Peng, X. Fan, S. Li, J. Zhang, Green synthesis and characterization of graphite oxide by orthogonal experiment, J. Chil. Chem. Soc. 58 (2013) 2213–2217, https://doi.org/10.4067/S0717-97072013000400067.

[40] K. Kobayashi, T. Hattori, Y. Honda, K. Kirimura, Oxalic acid production by citric acid-producing Aspergillus Niger overexpressing the oxaloacetate hydrolase gene oahA, J. Ind. Microbiol. Biotechnol. 41 (2014) 749–756, https://doi.org/10.1007/s10295-014-1419-2.
[41] H. Müller, L. Barthel, S. Schmideder, T. Schütze, V. Meyer, H. Briesen, From spores to fungal pellets: a new high-throughput image analysis highlights the structural development of Aspergillus Niger, Biotechnol. Bioeng. 119 (2022) 2182–2195, https://doi.org/10.1002/bit.28124.
[42] M. Shuler, F. Kargi, Bioprocess engineering: Basic Concepts, xvi (2002).
[43] Z.Y. Du, K. Zienkiewicz, N. Vande Pol, N.E. Ostrom, C. Benning, G.M. Bonito, Algal-fungal symbiosis leads to photosynthetic mycelium, Elife 8 (2019) 47815, https://doi.org/10.7554/eLife.47815.
[44] S.K. Prajapati, P. Kumar, A. Malik, P. Choudhary, Exploring pellet forming filamentous fungi as Tool for harvesting non-flocculating Unicellular microalgae, Bioenergy Res 7 (2014) 1430–1440, https://doi.org/10.1007/s12155-014-9481-1.
[45] H.A. El-Enshasy, Filamentous fungal Cultures-process characteristics, products, and applications, in: Bioprocessing for Value-Added Products from Renewable Resources: New Technologies and Applications, 2006, pp. 225–261, https://doi.org/10.1016/B978-044452114-9/50010-4.
[46] S.K. Wang, K.X. Yang, Y.R. Zhu, X.Y. Zhu, D.F. Nie, N. Jiao, I. Angelidaki, One-step co-cultivation and flocculation of microalgae with filamentous fungi to valorize starch wastewater into high-value biomass, Bioresour. Technol. 361 (2022) 127625, https://doi.org/10.1016/j.biortech.2022.127625.
[47] H. Yu, J. Kim, C. Lee, Nutrient removal and microalgal biomass production from different anaerobic digestion effluents with Chlorella species, Sci. Rep. 9 (2019) 1–13, https://doi.org/10.1038/s41598-019-42521-2.
[48] H. Bücking, A. Kafle, Role of arbuscular mycorrhizal fungi in the nitrogen uptake of plants: Current knowledge and research gaps, Agronomy 5 (2015) 587–612, https://doi.org/10.3390/agronomy5040587.
[49] Y. Su, Revisiting carbon, nitrogen, and phosphorus metabolisms in microalgae for wastewater treatment, Sci. Total Environ. 762 (2021) 144590, https://doi.org/10.1016/j.scitotenv.2020.144590.
[50] A. Solovchenko, I. Khozin-Goldberg, I. Selyakh, L. Semenova, T. Ismagulova, A. Lukyanov, I. Mamedov, E. Vinogradova, O. Karpova, I. Konyukhov, et al., Phosphorus starvation and luxury uptake in green microalgae revisited, Algal Res. 43 (2019) 101651, https://doi.org/10.1016/j.algal.2019.101651.
[51] S. Eixler, U. Karsten, U. Selig, Phosphorus storage in Chlorella vulgaris (Trebouxiophyceae, Chlorophyta) cells and its dependence on phosphate supply, Phycologia 45 (2006) 53–60, https://doi.org/10.2216/04-79.1.
[52] E.H. John, K.J. Flynn, Modelling phosphate transport and assimilation in microalgae; how much complexity is warranted? Ecol. Modell. 125 (2000) 145–157, https://doi.org/10.1016/S0304-3800(99)00178-7.
[53] S.F. Mohsenpour, S. Hennige, N. Willoughby, A. Adeloye, T. Gutierrez, Integrating micro-algae into wastewater treatment: a review, Sci. Total Environ. 752 (2021) 142168, https://doi.org/10.1016/j.scitotenv.2020.142168.
[54] E. Sanz-Luque, A. Chamizo-Ampudia, A. Llamas, A. Galvan, E. Fernandez, Understanding nitrate assimilation and its regulation in microalgae, Front. Plant Sci. 6 (2015) 00899, https://doi.org/10.3389/fpls.2015.00899.
[55] M. Hultberg, A.S. Carlsson, S. Gustafsson, Treatment of drainage solution from hydroponic greenhouse production with microalgae, Bioresour. Technol. 136 (2013) 401–406, https://doi.org/10.1016/j.biortech.2013.03.019.
[56] J. Peng, K. Kumar, M. Gross, T. Kunetz, Z. Wen, Removal of total dissolved solids from wastewater using a revolving algal biofilm reactor, Water Environ. Res. 92 (2020) 766–778, https://doi.org/10.1002/wer.1273.
[57] C. Lara, R. Rodriguez, M.G. Guerrero, Sodium-dependent nitrate transport and energetics of cyanobacteria, J. Phycol. 29 (1993) 389–395, https://doi.org/10.1111/j.1529-8817.1993.tb00139.x.
[58] E. Fernández, Á. Llamas, A. Galván, The Chlamydomonas Sourcebook: nitrogen assimilation. https://doi.org/10.1016/B978-0-12-370873-1.00011-3, 2009.
[59] T.A.V. Rees, R.C. Cresswell, P.J. Syrett, Sodium-dependent uptake of nitrate and urea by a marine diatom, BBA - Biomembr 596 (1980) 141–144, https://doi.org/10.1016/0005-2736(80)90178-9.
[60] Q. Wu, L. Guo, X. Li, Y. Wang, Effect of phosphorus concentration and light/dark condition on phosphorus uptake and distribution with microalgae, Bioresour. Technol. 340 (2021) 125745, https://doi.org/10.1016/j.biortech.2021.125745.
[61] W. Fricke, Glutamine synthetase and glutamate synthase activities in high ammonium grown wheat cells, Phytochemistry 34 (1993) 637–644, https://doi.org/10.1016/0031-9422(93)85331-K.
[62] R. Tischner, A. Schmidt, A Thioredoxin-mediated Activation of glutamine synthetase and glutamate synthase in Synchronous Chlorella sorokiniana, Plant Physiol 70 (1982) 113–116, https://doi.org/10.1104/pp.70.1.113.
[63] Y. Chisti, Biodiesel from microalgae beats bioethanol, Trends Biotechnol. 26 (2008) 126–131, https://doi.org/10.1016/j.tibtech.2007.12.002.
[64] R. Chu, S. Li, L. Zhu, Z. Yin, D. Hu, C. Liu, F. Mo, A review on co-cultivation of microalgae with filamentous fungi: efficient harvesting, wastewater treatment and biofuel production, Renew. Sustain. Energy Rev. 139 (2021) 110689, https://doi.org/10.1016/j.rser.2020.110689.
[65] H. Sun, W. Zhao, X. Mao, Y. Li, T. Wu, F. Chen, High-value biomass from microalgae production platforms: Strategies and progress based on carbon metabolism and energy conversion, Biotechnol. Biofuels 11 (2018) 227, https://doi.org/10.1186/s13068-018-1225-6.
[66] H. Peng, D. Wei, G. Chen, F. Chen, Transcriptome analysis reveals global regulation in response to CO2 supplementation in oleaginous microalga Coccomyxa subellipsoidea C-169, Biotechnol. Biofuels 9 (2016) 151, https://doi.org/10.1186/s13068-016-0571-5.
[67] J. Chen, W. Xu, Z. Wang, L. Tian, W. Liu, A. Ren, R. Liu, J. Zhu, L. Shi, Mitochondrial pyruvate carrier influences ganoderic acid biosynthesis in Ganoderma lucidum, Appl. Microbiol. Biotechnol. 107 (2023) 1361–1371, https://doi.org/10.1007/s00253-022-12357-4.
[68] S. Li, P. Xie, H. Chang, S.H. Ho, Simultaneously enhancement in the assimilation of microalgal nitrogen and the accumulation of carbohydrate by Debaryomyces hansenii, Chemosphere 336 (2023) 139183, https://doi.org/10.1016/j.chemosphere.2023.139183.
[69] E.W. Becker, Micro-algae as a source of protein, Biotechnol. Adv. 25 (2007) 207–210, https://doi.org/10.1016/j.biotechadv.2006.11.002.
[70] M.E.T. da Silva, M.A. Leal, M. de, O. Resende, M.A. Martins, J.S. dos, R. Coimbra, Scenedesmus obliquus protein concentrate: A sustainable alternative emulsifier for the food industry, Algal Res. 59 (2021) 102468. https://doi.org/10.1016/j.algal.2021.102468.
[71] P. Spolaore, C. Joannis-Cassan, E. Duran, A. Isambert, Commercial applications of microalgae, J. Biosci. Bioeng. 101 (2006) 87–96, https://doi.org/10.1263/jbb.101.87.
[72] M.G. Sajilata, R.S. Singhal, M.Y. Kamat, Fractionation of lipids and purification of γ-linolenic acid (GLA) from Spirulina platensis, Food Chem. 109 (2008) 580–586, https://doi.org/10.1016/j.foodchem.2008.01.005.
[73] A. Aneiros, A. Garateix, Bioactive peptides from marine sources: Pharmacological properties and isolation procedures, J. Chromatogr., B: Anal. Technol. Biomed. Life Sci. 803 (2004) 41–53, https://doi.org/10.1016/j.jchromb.2003.11.005.
[74] M.N. Kronick, P.D. Grossman, Immunoassay techniques with fluorescent phycobiliprotein conjugates, Clin. Chem. 29 (1983) 1582–1586, https://doi.org/10.1093/clinchem/29.9.1582.